Gastroenterology 2022;163:1281–1293

Acetyl-Coenzyme A Synthetase 2 Potentiates Macropinocytosis and Muscle Wasting Through Metabolic Reprogramming in Pancreatic Cancer

Zhijun Zhou,[1,2,*] **Yu Ren**,[1,2,*] **Jingxuan Yang**,[1,2,*] **Mingyang Liu**,[1,2,*] **Xiuhui Shi**,[1,2,*] Wenyi Luo,[3] Kar-Ming Fung,[3] Chao Xu,[4] Michael S. Bronze,[1] Yuqing Zhang,[1,2] Courtney W. Houchen,[1] and Min Li[1,2]

[1]Department of Medicine, the University of Oklahoma Health Sciences Center, Oklahoma City, Oklahoma; [2]Department of Surgery, the University of Oklahoma Health Sciences Center, Oklahoma City, Oklahoma; [3]Department of Pathology, the University of Oklahoma Health Sciences Center, Oklahoma City, Oklahoma; and [4]Department of Biostatistics and Epidemiology, Hudson College of Public Health, the University of Oklahoma Health Sciences Center, Oklahoma City, Oklahoma

GI CANCER

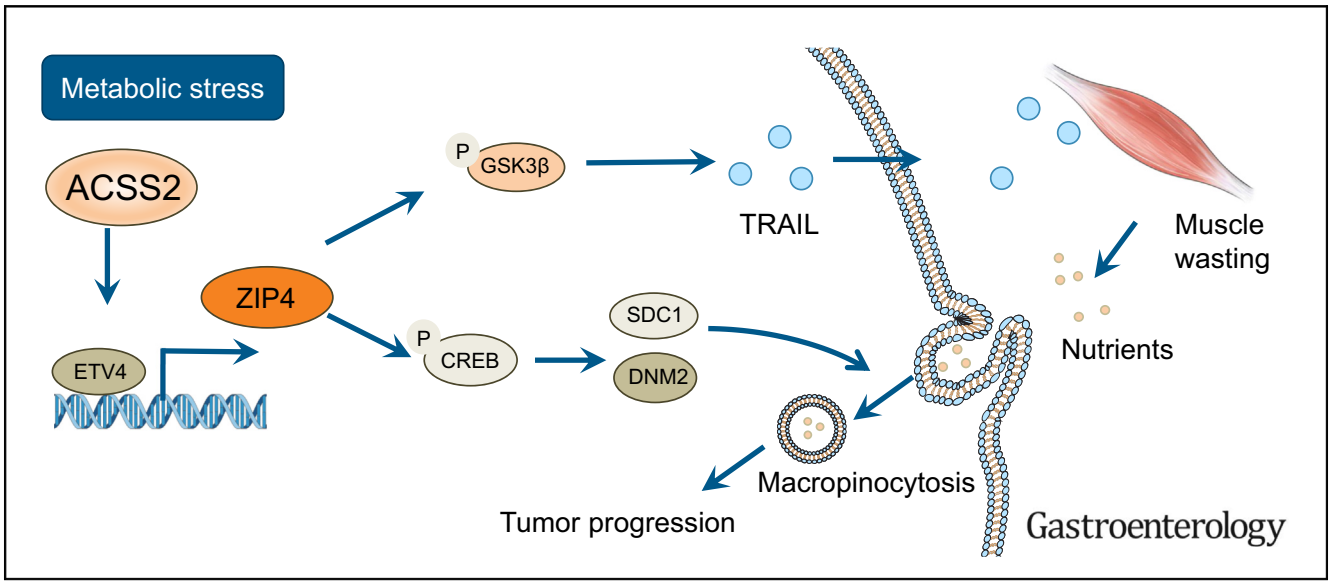

See editorial on page 1161.

BACKGROUND & AIMS: Rapid deconditioning, also called cachexia, and metabolic reprogramming are two hallmarks of pancreatic cancer. Acetyl-coenzyme A synthetase short-chain family member 2 (ACSS2) is an acetyl-enzyme A synthetase that contributes to lipid synthesis and epigenetic reprogramming. However, the role of ACSS2 on the nonselective macropinocytosis and cancer cachexia in pancreatic cancer remains elusive. In this study, we demonstrate that ACSS2 potentiates macropinocytosis and muscle wasting through metabolic reprogramming in pancreatic cancer. **METHODS:** Clinical significance of ACSS2 was analyzed using samples from patients with pancreatic cancer. ACSS2-knockout cells were established using the clustered regularly interspaced short palindromic repeats-associated protein 9 system. Single-cell RNA sequencing data from genetically engineered mouse models was analyzed. The macropinocytotic index was evaluated by dextran uptake assay. Chromatin immunoprecipitation assay was performed to validate transcriptional activation. ACSS2-mediated tumor progression and muscle wasting were examined in orthotopic xenograft models. **RESULTS:** Metabolic stress induced ACSS2 expression, which is associated with worse prognosis in pancreatic cancer. ACSS2 knockout significantly suppressed cell proliferation in 2-dimensional and 3-dimensional models. Macropinocytosis-associated genes are upregulated in tumor tissues and are correlated with worse prognosis. ACSS2 knockout inhibited macropinocytosis. We identified Zrt- and Irt-like protein 4 (ZIP4) as a downstream target of ACSS2, and knockdown of ZIP4 reversed ACSS2-induced macropinocytosis. ACSS2 upregulated ZIP4 through ETV4-mediated transcriptional activation. ZIP4 induces macropinocytosis through cyclic adenosine monophosphate response element-binding protein–activated syndecan 1 (SDC1) and dynamin 2 (DNM2). Meanwhile, ZIP4 drives muscle wasting and cachexia via glycogen synthase kinase-β (GSK3β)–mediated secretion of tumor necrosis factor superfamily member 10 (TRAIL or TNFSF10). ACSS2 knockout attenuated muscle wasting and extended survival in orthotopic mouse models. **CONCLUSIONS:** ACSS2-mediated metabolic reprogramming

activates the ZIP4 pathway, and promotes macropinocytosis via SDC1/DNM2 and drives muscle wasting through the GSK3β/TRAIL axis, which potentially provides additional nutrients for macropinocytosis in pancreatic cancer.

Keywords: Cachexia; Macropinocytosis; Metabolic Stress; Muscle Wasting.

Rapid deconditioning, also known as cancer cachexia, is a systemic dysfunction characterized by uncontrollable body weight loss independent of nutritional supplement.[1,2] Muscle wasting, adipose loss, and loss of appetite (anorexia) are prevalent in those patients. Cachexia is associated with multiorgan dysfunction and increased mortality.[1,3] Currently, no effective treatment options have been approved to reverse or ameliorate cancer cachexia.[4] Novel therapeutic targets and treatment strategies are urgently needed. Pancreatic cancer has the highest prevalence of cachexia among all cancer types, highlighting its unique pathologic alterations for the development of cachexia.[1,5]

Pancreatic cancer is characterized with desmoplasia, which creates a hypoxic, acidic, and nutrient-deficient microenvironment compared with adjacent benign pancreas tissue.[6,7] However, the mechanism of pancreatic cancer cells surviving in this nutrient deficiency remains elusive. Cancer cells develop multiple ways to overcome the metabolic stress induced by the hazard tumor microenvironment, such as increasing lipogenesis and nutrient uptake. Oncogenic *RAS* mutant tumor cells depend on protein scavenging to maintain tumor fitness in the nutrient-deficient microenvironment, a process known as macropinocytosis.[8] Because most pancreatic cancer has a Kirsten rat sarcoma viral oncogene homolog (KRAS) mutation, macropinocytosis represents a critical source of amino acid supply for this devastating disease. Nonetheless, how pancreatic cancer cells coordinate between cachexia and macropinocytosis remains poorly defined.

Acyl-coenzyme A synthetase short-chain family member 2 (ACSS2) is an enzyme responsible for converting acetate into acetyl- coenzyme A, which contributes to energy production and lipogenesis. It has been reported that ACSS2 helps tumor cells survive metabolic stress by reprogramming metabolic profiles in several tumor types, such as breast cancer and glioblastoma.[9,10] Acidic microenvironment can induce ACSS2 expression via sterol regulatory element-binding proteins (SREBPs) in pancreatic cancer.[11] Pancreatic intraepitheliel neoplasia lesions and pancreatic cancer tissue also showed high expression of ACSS2.[12] Nevertheless, the role of ACSS2 on regulating metabolic stress and cancer cachexia in pancreatic cancer is unknown.

In this study, we found that metabolic stress can induce ACSS2 expression. Meanwhile, ACSS2 is upregulated in pancreatic cancer tissues, especially at the regions where tumor cells suffer from metabolic stress, such as the necrotic area. ACSS2 promotes macropinocytosis to maintain the supply of amino acids for tumor growth. ACSS2 upregulates macropinocytosis in an erythroblast transformation specific variant transcription factor 4 (ETV4)/Zrt- and Irt-like protein 4 (ZIP4)–dependent manner via , syndecan 1 (SDC1) and dynamin 2 (DNM2). Furthermore, ZIP4 promotes muscle wasting through the glycogen synthase kinase 3 (GSK3)β/tumor necrosis factor superfamily member 10 (TRAIL) axis, resulting in cancer cachexia, which potentially provides nutrients to maintain tumor fitness. ACSS2 dominates the

WHAT YOU NEED TO KNOW

BACKGROUND AND CONTEXT

Cachexia and metabolic reprogramming are two hallmarks of pancreatic cancer. Acetyl-coenzyme A synthetase 2 (ACSS2) is an acetyl-coA synthetase that contributes to lipid synthesis and epigenetic reprogramming. The study demonstrates that ACSS2 potentiates macropinocytosis and muscle wasting through metabolic reprogramming in pancreatic cancer.

NEW FINDINGS

ACSS2 promotes metabolic reprogramming through erythroblast transformation specific variant transcription factor 4 (ETV4)/Zrt- and Irt-like protein 4 (ZIP4) pathway, whereby ZIP4 promotes macropinocytosis via syndecan 1 (SDC1)/dynamin 2 (DNM2) and drives muscle wasting through the glycogen synthase kinase 3-β/tumor necrosis factor superfamily member 10 (TRAIL) pathway, which in turn provides additional nutrients for macropinocytosis in pancreatic cancer.

LIMITATIONS

This study was performed in cell lines and mouse models. Further studies are needed to validate the results in patients.

IMPACT

This study identifies ACSS2 as a key regulator that potentiates macropinocytosis and muscle wasting through metabolic reprogramming, thus representing an attractive therapeutic target to attenuate cachexia in pancreatic cancer.

*** Authors share co-first authorship.**

Abbreviations used in this paper: **3D, 3-dimensional; ACSS2, acetyl-coenzyme A synthetase short-chain family member 2; AKT, protein kinase B; Cas9, CRISPR associated protein 9; ChIP, chromatin immunoprecipitation; CREB, cyclic adenosine monophosphate response element-binding protein; CRISPR, clustered regularly interspaced short palindromic repeats; DNM2, dynamin 2; EdU, 5-ethynyl-2'-deoxyuridine; ETV4, erythroblast transformation specific variant transcription factor 4; FBS, fetal bovine serum; FGF, fibroblast growth factor; GSK3, glycogen synthase kinase 3; H3K27ac, histone H3 lysine 27 acetylation; IL, interleukin; KLF16, Kruppel like factor 16; KO, knockout; KRAS, Kirsten rat sarcoma viral oncogene homolog; mRNA, messenger RNA; MuRF1, tripartite motif containing 63; PBS, phosphate-buffered saline; PCR, polymerase chain reaction; SDC1, syndecan 1; SREBP, sterol regulatory element-binding protein; TCGA, The Cancer Genome Atlas; TGF, transforming growth factor; TRAIL, tumor necrosis factor superfamily member 10; ZIP4, Zrt- and Irt-like protein 4.**

Most current article

0016-5085/$36.00
https://doi.org/10.1053/j.gastro.2022.06.058

metabolic reprogramming by orchestrating macropinocytosis and muscle wasting to support tumor progression in pancreatic cancer. Targeting ACSS2 holds the promise for retarding the development of cancer cachexia in pancreatic cancer.

Materials and Methods

Cell Lines and Plasmids

Pancreatic cancer cell lines and C2C12 cells were obtained from American Type Culture Collection (Rockville, MD), and were maintained in RPMI 1640 medium or Iscove's Modified Dulbecco's Medium or Dulbecco's Modified Eagle Medium supplemented with 10% fetal bovine serum (FBS). All cell lines have been authenticated and evaluated as mycoplasma free. hACSS2 plasmid (EX-Z9293-Lv217) and the empty control vector (EX-NEG-Lv217) were purchased from GeneCopoeia (Rockville, MD). The eSpCas9(1.1) (Plasmid #71814), lenti single guide RNA (MS2)_puro optimized backbone (Plasmid #73797), pLX_TRC311 (Plasmid #113668), and pLX_TRC311 ETV4-L (Plasmid #74982) were obtained from Addgene (Watertown, MA).

Clustered Regularly Interspaced Short Palindromic Repeats-Associated Protein 9

ACSS2-knockout (KO) cell lines were established using the clustered regularly interspaced short palindromic repeats (CRISPR)-CRISPR associated protein 9 (Cas9) system.[13] Cas9-overexpression cell lines were established with the eSpCas9(1.1) (Plasmid #71814, Addgene). The guide RNA oligonucleotides that target ACSS2 were cloned into the single guide RNA MS2 backbone plasmid (Plasmid #73797) using the Gibson Assembly (New England BioLabs, Ipswich, MA).[14] The plasmids were collected with the Plasmid DNA Maxiprep Kit (Invitrogen, Carlsbad, CA) and validated by sequencing. The plasmids were then introduced into the Cas9-overexpression cell lines. Monocolonies of ACSS2-KO cells were selected.

Chromatin Immunoprecipitation

Chromatin immunoprecipitation (ChIP) was performed using the MAGnify Chromatin Immunoprecipitation System (Invitrogen) according the manufacturer's instruction. Briefly, cell pellets were crosslinked with formaldehyde, followed by lysing the cells and shearing the chromatin, which was then diluted and incubated with antibody-incorporated beads. The chromatin was washed, followed by reverse crosslinking and DNA purification. The purified DNA was then used for polymerase chain reaction (PCR).

Construction of Stable Cell Lines

Stable cell lines were constructed as previously described.[15,16] Briefly, plasmids were amplified in Stbl3 competent *Escherichia coli* cells and then collected by the Plasmid DNA Maxiprep Kit (Invitrogen). Plasmids of interest, together with psPAX2 (#12260, Addgene) and VSV-G (#8454, Addgene) plasmids were transfected into 293Ta cells by Lipofectamine 3000 (#L3000015, Invitrogen). After 48 to 72 hours, the supernatant was collected and filtered for the transfection of cells. The stable cells were selected with puromycin, followed by single colony isolation.

Three-Dimensional Spheroid Model

The 3-dimensional (3D) spheroid model was constructed as previously described.[15,16] Briefly, tumor cells were resuspended in culture medium with 0.24% methylcellulose and seeded as 20-μL droplets in the inner lid of a 10-cm dish, which was filled with 10 mL phosphate buffer solution. The spheroids were allowed to grow in 5% CO_2 at 37°C. Images were taken at different times to monitor the size of the spheroids.

Western Blot Analysis

Western blot was performed as previously described.[17] Cell lysates were loaded onto sodium dodecyl sulfate–polyacrylamide gel for electrophoresis. After the electrophoresis, the protein was transferred onto nitrocellulose membrane and blocked in 5% skim milk at room temperature for 1 hour, followed by the incubation with desirable antibodies against ZIP4 (1:2000; Proteintech, Rosemont, IL), ACSS2 (1:1000; Santa Cruz Biotechnology, Dallas, TX), ACTB (1:10000; Proteintech), MuRF1 (1:500; R&D Systems, Inc, Minneapolis, MN), atrogin-1 (1:1000; ECM Biosciences, Versailles, KY), myosin heavy chain (1:1000; University of Iowa, Iowa City, IA), SDC1 (Proteintech, 1:1000), phosphorylated GSK3β (1:1000; Cell Signaling Technology, Danvers, MA), total GSK3β (1:1000; Cell Signaling Technology), phosphorylated cyclic adenosine monophosphate response element-binding protein (CREB) (1:1000; Cell Signaling Technology), total CREB (1:1000; 1:1000), ETV4 (1:1000; Aviva Systems Biology, San Diego, CA), or mouse ZIP4 (1:1000; R&D) at 4°C overnight. The membrane was washed with Tris-buffered saline buffer with 0.1% Tween 20, followed by the incubation of IRDye secondary antibodies (1:10,000) at room temperature for 2 hours. The results were examined by Odyssey Imager (LI-COR Biotechnology, Lincoln, NE).

5-Ethynyl-2'-Deoxyuridine Incorporation Assay

The 5-ethynyl-2'-deoxyuridine (EdU) incorporation assay was performed using the Click-iT EdU Cell Proliferation Kit (#C10339, Thermo Fisher Scientific, Waltham, MA), following the manufacturer's instructions. Tumor cells were seeded on the chamber slides and allowed to grow overnight. Cells were then cultured with medium containing EdU (10 μmol/L) for 3 to 4 hours and fixed by 3.7% formaldehyde in phosphate-buffered saline (PBS) for 15 minutes at room temperature, followed by permeabilization with 0.5% Triton X-100 before being incubated with Click-iT reaction cocktail at room temperature for 30 minutes, followed by DNA staining with Hoechst at room temperature for 20 to 30 minutes. The images were captured by an Olympus Fluorescence Microscope (Olympus, Waltham, MA).

Quantitative Reverse-Transcription Polymerase Chain Reaction

RNA was purified by the PureLink RNA Mini Kit (#12183025, Thermo Fisher Scientific) and complementary DNA was obtained using the complementary DNA Reverse

Transcription Kit (#4368814, Thermo Fisher Scientific), following the manufacturer's instructions. PowerUp SYBR Green Master Mix (#4367659, Thermo Fisher Scientific) was used for quantitative PCR by the LightCycler 96 Instrument (Roche Diagnostics Corp, Indianapolis, IN). Primers used for reverse-transcription quantitative PCR are listed in Supplementary Table 1.

MTT Assay

Cells were seeded in 96-well plate at desirable density and allowed to grow overnight. Culture medium was then removed, and each well was added with alamarBlue (Bio-Rad, Hercules, CA) and cultured at 37°C for 2 hours, according to the manufacturer's instructions. Results were examined with a microplate reader (BioTek, Broadview, IL).

Pancreatic Cancer Orthotopic Xenograft Mouse Model

The study used athymic nude male mice aged 5 to 6 weeks. All mice were cared for according to the study protocol approved by the University of Oklahoma Health Sciences Center Animal Welfare Committee. ASPC-Cas9, ASPC-ACSS2–KO, CFPAC-Cas9, and CFPAC-ACSS2–KO stable cell lines were used to establish the orthotopic xenograft pancreatic cancer model. Briefly, tumor cells were trypsinized and resuspended in RPMI 1640 or Iscove's Modified Dulbecco's Medium at a density of 6×10^7 cells/mL. The mice were maintained with isoflurane anesthesia during surgery. Surgical aseptic technique was applied for the construction of the model. Each mouse was injected with a 50-μL cell suspension containing 3×10^6 pancreatic cancer cells into the pancreas. The wound was sutured with Vicryl 4-0 (Ethicon, Somerville, NJ). The mice were euthanized after 5 to 6 weeks for tissue collection. For survival analysis, mice were carefully monitored and euthanized when they were moribund or reached the end point of the study protocol.

Dextran Uptake Assay

Dextran uptake assay was performed to evaluate macropinocytosis.[18] Briefly, cells were seeded on chamber slides at the desirable density and allowed to grow for 24 to 48 hours, followed by the starvation in culture medium with 0.1% FBS for 24 hours. Cells were treated with 1 mg/mL dextran (#D1818, Thermo Fisher Scientific) at 37°C for 1 hour, followed by PBS wash and fixation with 3.7% formaldehyde for 30 minutes at room temperature. After nuclei staining with Hoechst at room temperature for 20 to 30 minutes, images were captured by an Olympus Fluorescence Microscope and analyzed by ImageJ software (National Institutes of Health, Bethesda, MD).

Immunohistochemistry

Tissues were fixed in formalin and embedded in paraffin, followed by sectioning into 4-μm-thick slides. Staining was performed as previously described. Briefly, the slides were deparaffinized, followed by antigen retrieval in citrate-based solution. The endogenous peroxidase was quenched in 3% H_2O_2 at room temperature for 10 minutes, followed by blocking with 2.5% horse serum. The sections were incubated in primary antibody at 4°C overnight, followed by incubation with horseradish peroxidase horse anti-rabbit IgG antibody for 30 minutes and 3,3′-diaminobenzidine tetra hydrochloride substrate for ~1 minute at room temperature. Hematoxylin QS was used for nuclear staining. The slides were dehydrated, mounted, and evaluated under a phase-contrast microscope. The cross-sectional areas of muscle fibers were analyzed in ImageJ.

Statistical Analysis

All of the analyses were performed in R 4.1.1 (R Foundation of Statistical Computing, Vienna, Austria) and GraphPad Prism 9.0 software (GraphPad Software, San Diego, CA). The unpaired 2-tailed Student test was applied for 2-group comparison, unless otherwise indicated. Survival data was analyzed using the log-rank test. Statistical significance was determined by P value $< .05$.

Results

Metabolic Stress Induces ACSS2 Expression, Which Promotes Cell Proliferation

The microenvironment of pancreatic cancer is characterized with metabolic stress induced by nutrient deficiency and hypoxia. We found that nutrient deficiency increased ACSS2 expression in pancreatic cancer cells (Figure 1*A* and Supplementary Figure 1*A*). Pancreatic cancer tissues also showed higher level of ACSS2 expression compared with normal pancreas tissues (Figure 1*B* and Supplementary Figure 1*B*). Higher ACSS2 expression is associated with worse overall survival in patients with pancreatic cancer (Supplementary Figure 1*C*). To further examine the function of ACSS2, we established the ACSS2-KO and ACSS2-overexpression pancreatic cancer cell lines, including AsPC-1 (cachectic) and CFPAC-1 (noncachectic) cells (Supplementary Figure 1*D* and *E*). The EdU incorporation assay showed that the DNA synthesis rate was decreased in ACSS2-KO cells and increased in ACSS2-overexpressed cells (Figure 1*C*).

Knockdown of mouse ACSS2 in *Kras*^{G12D} *Trp53*^{R172H}*Pdx1-Cre* (KPC) cells also decreased DNA synthesis (Figure 1*D* and Supplementary Figure 1*F*). We found that ACSS2 KO decreased cell proliferation and colony formation, whereas ACSS2 overexpression increased cell proliferation in human pancreatic cancer cells (Figure 1*E* and *F* and Supplementary Figure 1*G* and *H*). Transient and stable knockdown of ACSS2 in pancreatic cancer cells also resulted in decreased cell proliferation (Supplementary Figure 1*I*). Furthermore, we established the 3D spheroid model and found that ACSS2 KO decreased the size of spheroids, whereas ACSS2 overexpression increased the size of spheroids (Figure 1*G* and *H* and Supplementary Figure 1*J*). These results indicate that metabolic stress induced ACSS2 expression and that ACSS2 KO suppressed cell proliferation in pancreatic cancer.

ACSS2 Upregulates Macropinocytosis in Pancreatic Cancer Progression

Emerging evidence showed that metabolic stress can upregulate macropinocytosis, a nonselective protein-scavenging process that grants tumor cells growth advantage in nutrient limitation. We analyzed single-cell RNA sequencing data (GSE125588) to evaluate the expression of

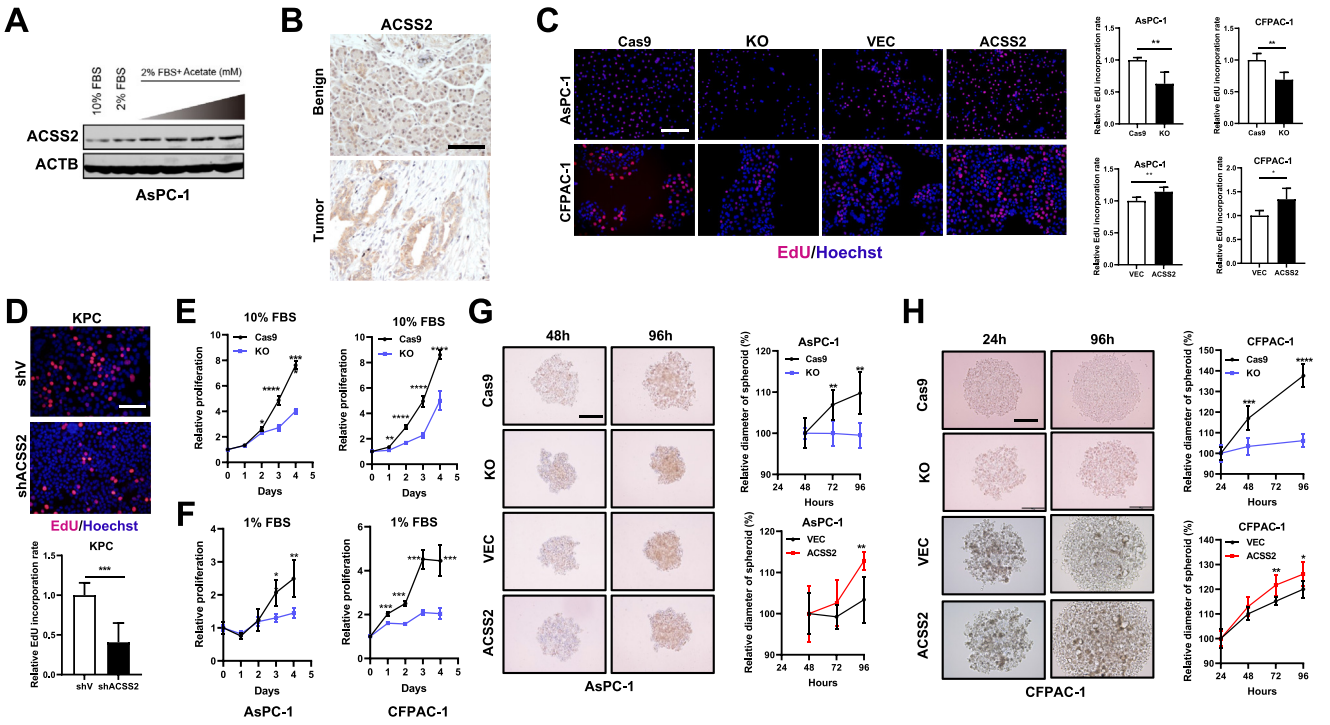

Figure 1. Metabolic stress induces ACSS2 expression and promotes cell proliferation. (*A*) ACSS2 expression of AsPC-1 cells treated with complete medium, 2% serum medium, and 2% serum medium supplemented with gradient concentration of sodium acetate for 72 hours. (*B*) ACSS2 expression in human pancreatic cancer tissues and benign pancreas tissues. The *scale bar* is 50 μm. (*C*) DNA synthesis rate was assessed by EdU incorporation assay in ACSS2-KO or ACSS2-overexpression cell lines. VEC, vector. The *scale bar* is 100 μm. (*D*) DNA synthesis rate was assessed by EdU incorporation assay in ACSS2-knockdown KPC cells. sh, short hairpin, The *scale bar* is 50 μm. Cell proliferation was assessed by MTT assay in ACSS2-KO cell lines in (*E*) complete medium (10% FBS) or (*F*) medium with 1% FBS. (*G* and *H*) Relative size of spheroids established from ACSS2-KO or ACSS2-overexpression cell lines. The *scale bar* is 200 μm. $^{*}P < .05$, $^{**}P < .01$, $^{***}P < .001$, $^{****}P < .0001$.

macropinocytosis-associated genes (*Sdc1*, *Dnm2*, *Snx33*, *Pycard*, *Lrrc16a*, and Appl2) in the pancreas of normal mice as well as several genetically engineered mouse models of pancreatic cancer, including early-stage (40 days) and late-stage (60 days) *KIC* and *KPC* mouse models. We found that the level of macropinocytosis-associated genes was increased during tumor progression (Supplementary Figures 2 and 3). We then evaluated the expression of those genes in human pancreatic cancer tissues and found that the expression of these macropinocytosis-associated genes was increased in pancreatic tumor tissues compared with adjacent benign tissues (Figure 2*A* and Supplementary Figure 4*A*–*C*).

ACSS2 expression is positively associated with macropinocytosis gene expression in cancer cells in the Cancer Cell Line Encyclopedia database and in patients with pancreatic cancer (Supplementary Figure 4*D*). The upregulation of these genes was associated with worse overall survival in patients with pancreatic cancer (Supplementary Figure 4*E*–*G*). This prompted us to investigate whether ACSS2 promotes pancreatic cancer progression by upregulating macropinocytosis. We further examined the uptake of dextran (70 kDa) in AsPC-1 and CFPAC-1 cells (Figure 2*B*) and found that ACSS2 KO decreased dextran uptake, whereas ACSS2 overexpression increased dextran uptake. Furthermore, knockdown of ACSS2 expression decreased dextran uptake in KPC cells (Figure 2*C*).

Overexpression of ACSS2 increased the messenger (m) RNA levels of several macropinocytosis-associated genes, including *SDC1*, *DNM2*, *SNX33*, *PYCARD*, *LRRC16A*, and *APPL2* in AsPC-1 and CFPAC-1 cells. ACSS2 KO did not affect the expression of *LRRC16A* in AsPC-1 cells and *SNX33* in CFPAC-1 cells, respectively (Figure 2*D* and *E*). *APPL2* and *PYCARD* genes were not upregulated in tumor tissues compared with the benign tissues. Therefore, we focused on SDC1 and DNM2 in the subsequent study.

To examine the impact of metabolic stress on SDC1 and DNM2, pancreatic cancer cells were cultured in normal condition (indicated as 10% FBS hereafter) or nutrient stress condition (indicated as 1% FBS hereafter). We found that nutrient stress increased the expression of ACSS2, SDC1, and DNM2. Knockout of ACSS2 decreased the expression of SDC1 and DNM2 (Figure 2*F* and *G* and Supplementary Figure 5*A*–*D*). Overexpression of ACSS2 upregulates SDC1 and DNM2 (Supplementary Figure 5*E*–*G*). These findings suggest that metabolic stress induces ACSS2, which upregulates macropinocytosis through SDC1 and DNM2.

ACSS2 Promotes Macropinocytosis Through ZIP4

To identify the downstream target of ACSS2 that mediates macropinocytosis, we analyzed the transcriptomic data of pancreatic cancer tissues in The Cancer Genome Atlas

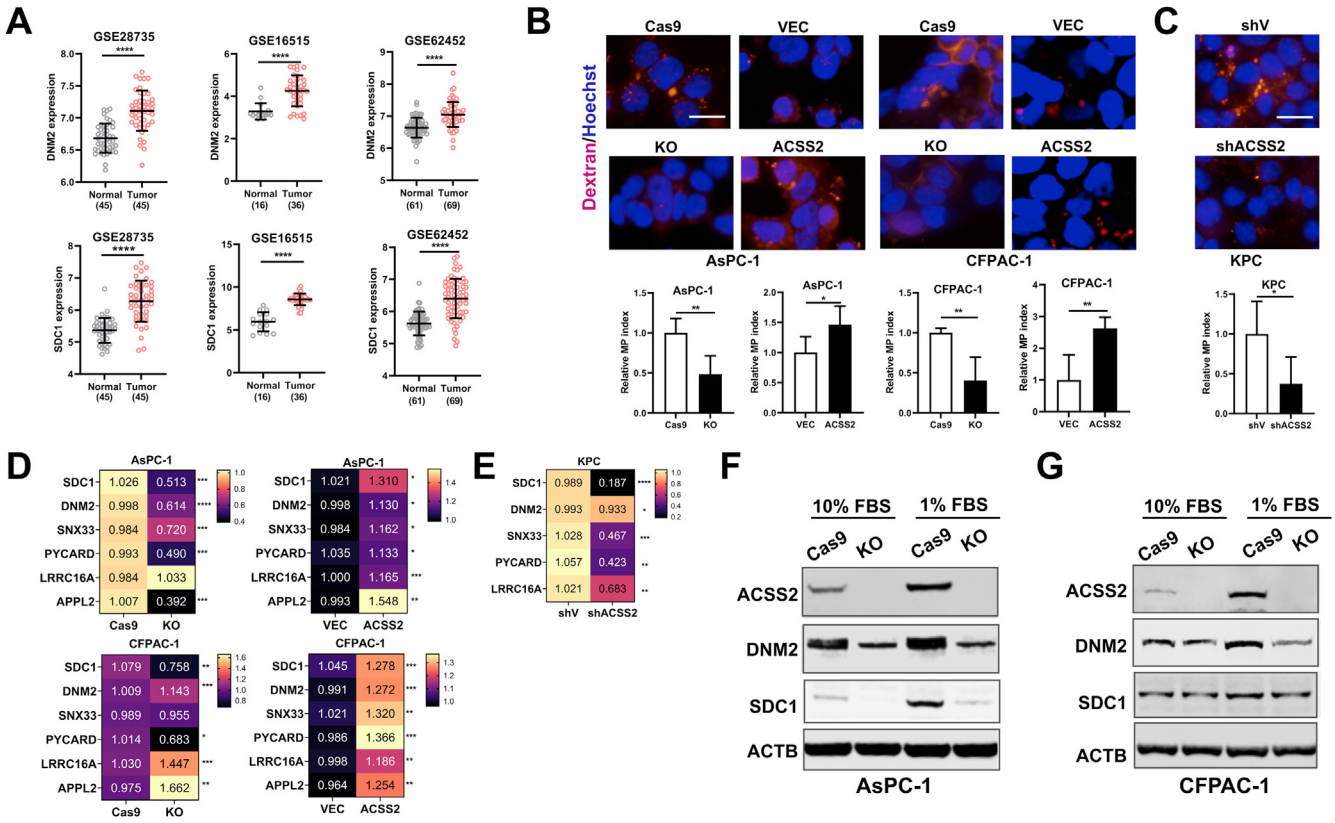

Figure 2. ACSS2 upregulates macropinocytosis in pancreatic cancer progression. (*A*) Expression level of DNM2 and SDC1 in pancreatic cancer cohorts. (*B*) Dextran uptake assay to assess macropinocytosis index in ACSS2-KO and ACSS2-overexpression human cell lines. The *scale bar* is 10 μm. (*C*) Dextran uptake assay to assess macropinocytosis index in ACSS2-knockdown KPC cells. sh, short hairpin. The *scale bar* is 10 μm. The mRNA level of macropinocytosis-associated genes in (*D*) ACSS2-KO and ACSS2-overexpression human cell lines and in (*E*) ACSS2-knockdown KPC cell line. (*F* and *G*) The protein level of macropinocytosis associated genes in ACSS2-KO cell lines cultured in normal condition or stress condition. *$P < .05$, **$P < .01$, ***$P < .001$, ****$P < .0001$.

(TCGA) data set. By comparing the differentially expressed genes between ACSS2-low and ACSS2-high tumors, we identified a subset of genes that are positively correlated with ACSS2 expression in pancreatic cancer (Supplementary Figure 6*A*). Among these candidates, we are particularly interested in ZIP4, a zinc importer that plays critical roles in cancer metastasis, chemoresistance, and cachexia in pancreatic cancer. We found that ZIP4 expression is higher in pancreatic cancer tissues compared with benign pancreas tissues (Supplementary Figure 6*B*). ZIP4 expression is positively correlated to ACSS2 expression in multiple pancreatic cancer cohorts (GSE16515, GSE28735, TCGA) and in cancer cell lines in the Cancer Cell Line Encyclopedia data set (Figure 3*A*–*C* and Supplementary Figure 6*C* and *D*). ACSS2 KO decreased ZIP4 expression, whereas ACSS2 overexpression upregulated ZIP4 expression in human pancreatic cancer cell lines (Figure 3*D*–*F* and Supplementary Figure 6*E and F*). We also validated these findings in KPC cell lines (Figure 3*G* and Supplementary Figure 6*G and H*). Then, we evaluated whether ACSS2 promotes macropinocytosis through ZIP4. We knocked down ZIP4 expression in ACSS2-overexpressed pancreatic cancer cells and found that it decreased the expression of macropinocytosis associated gene profiles (Supplementary Figure 6*I*).

These findings prompted us to evaluate whether ACSS2 increased cell proliferation through ZIP4-mediated macropinocytosis. ZIP4 knockdown in ACSS2-overexpressed pancreatic cancer cells suppressed dextran uptake in the normal condition and stress condition (Figure 3*H* and *I*). Meanwhile, knockdown of ZIP4 reversed the upregulated DNA synthesis rate induced by ACSS2 overexpression (Figure 3*J* and *K*). Dependency score analysis showed that KO of ZIP4 suppressed proliferation of pancreatic cancer cells (Supplementary Figure 6*J*). ZIP4, in combination with macropinocytosis-associated genes, such as *SDC1* and *DNM2*, can better stratify patients with different prognoses (Supplementary Figure 6*K* and *L*). Together, these results demonstrate ACSS2 promotes macropinocytosis through ZIP4.

ACSS2 Upregulates ZIP4 Through ETV4

To identify the putative transcription factors that mediate ACSS2-upregulated ZIP4 expression, we analyzed the pancreatic cancer tissue samples in TCGA database and found 6450 ZIP4-correlated genes ($P < .001$) and 4530 ACSS2-correlated genes ($P < .001$). We also analyzed the JASPAR database (https://jaspar.genereg.net/) and the

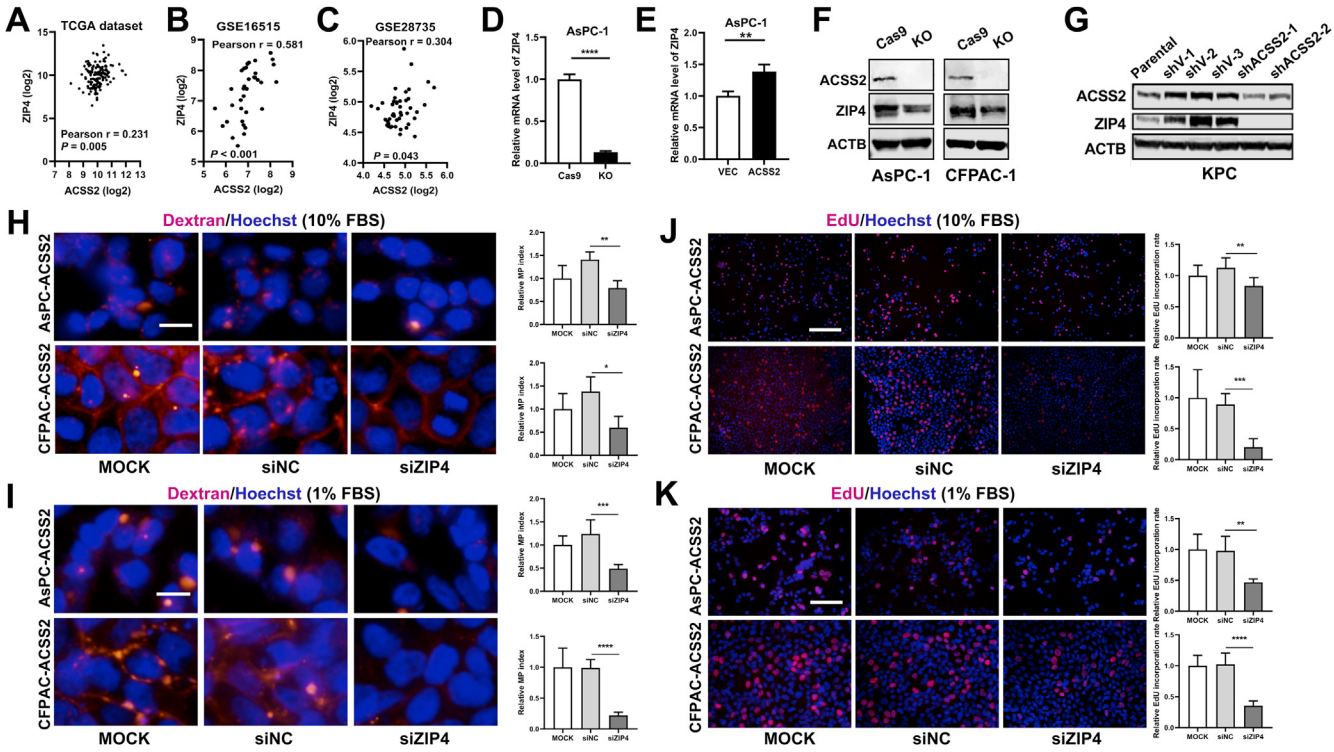

Figure 3. ACSS2 promotes macropinocytosis through ZIP4. Correlation between ACSS2 and ZIP4 expression in (*A*) TCGA cohort. (*B*) GSE16515 cohort, and (*C*) GSE28735 cohort. mRNA level of ZIP4 in (*D*) ACSS2-KO or (*E*) ACSS2-overexpression cell lines. VEC, vector. (*F*) Protein level of ZIP4 in ACSS2-KO cell lines. (*G*) Protein levels of ZIP4 in ACSS2 knockdown KPC cells. sh, short hairpin. Dextran uptake assay to assess macropinocytosis index in ACSS2-overexpression cell lines with ZIP4 knockdown in (*H*) 10% FBS or (*I*) 1% FBS. The *scale bar* is 10 μm. (*J* and *K*) DNA synthesis rate was assessed by EdU incorporation assay in ACSS2-overexpression cell lines transfected with small interfering (si) negative control (NC) or siZIP4 siRNA in normal condition or under metabolic stress. The *scale bars* are 100 μm and 50 μm respectively. $^{*}P < .05$, $^{**}P < .01$, $^{***}P < .001$, $^{****}P < .0001$.

University of California Santa Cruz Genome Browser and identified 47 potential transcription factors for ZIP4. Then, we merged these gene clusters and got the consensus genes that serve as the potential transcription factors for ZIP4, including *ETV4*, *MEF2C*, *IKZF1*, *KLF9*, *ZNF135*, *ZBTB6*, *KLF16*, *SMAD2*, *MEF2A*, *GATA2*, *KLF5*, *ZNF148*, and *GLI3*. Among these transcription factors, ETV4, KLF16, and KLF5 are positively correlated with ACSS2 (Figure 4*A*).

We are interested in ETV4 and KLF16, which play critical roles in promoting pancreatic cancer progression. Knockdown of ACSS2 decreased the mRNA level of ETV4 and KLF16 (Figure 4*B*). Then, we examined the expression level of these 2 transcription factors in pancreatic cancer tissues and normal tissues. We found that only ETV4 but not KLF16 was increased in pancreatic cancer tissues compared with normal pancreas tissues (Supplementary Figure 7*A*–*F*). ETV4 is associated with ACSS2 and ZIP4 expression in patients' tumor tissues (Supplementary Figure 7*G* and *H*). We found that ETV4 overexpression can increase the mRNA level of ZIP4 in pancreatic cancer cells (Figure 4*C* and Supplementary Figure 7I).

To further validate that ETV4 can transcriptionally activate ZIP4, we analyzed the promoter region of ZIP4 and identified 2 potential binding motifs of ETV4. We performed ChIP using ETV4 antibody and found that ETV4 can bind to the promoter region of ZIP4 (Figure 4*D* and Supplementary Figure 7*J*). Overexpression of ACSS2 upregulated ETV4. We further validated that loss of ACSS2 reduced metabolic stress–induced upregulation of ETV4 (Figure 4*E* and *F* and Supplementary 7*K* and *L*).

To further investigate the role of ETV4 in this signaling axis, we examined the histone H3 lysine 27 acetylation (H3K27ac) on the enhancer or promoter region, which can activate gene expression.[19] ACSS2 can directly regulate histone acetylation.[20] To explore whether ACSS2 upregulates ETV4 through H3K27ac modification on the promoter region of ETV4, we performed ChIP-PCR assay and demonstrated that ACSS2 increases H3K27ac modification on the promoter region of ETV4 and that when ACSS2 was knocked out, the level of H3K27ac modification on the promoter region of ETV4 was decreased (Supplementary Figure 7M). These findings demonstrate that ACSS2 upregulates ZIP4 through ETV4, via H3K27ac modification.

ACSS2 Promotes Macropinocytosis Through ZIP4/Cyclic Adenosine Monophosphate Response Element-Binding Protein Pathway

ACSS2 induced the expression of ZIP4 and phosphorylation of GSK3β and CREB, while ACSS2 KO decreased ZIP4 expression and phosphorylation of GSK3β and CREB (Figure 4*E* and *F* and Supplementary Figure 7K and *L*).

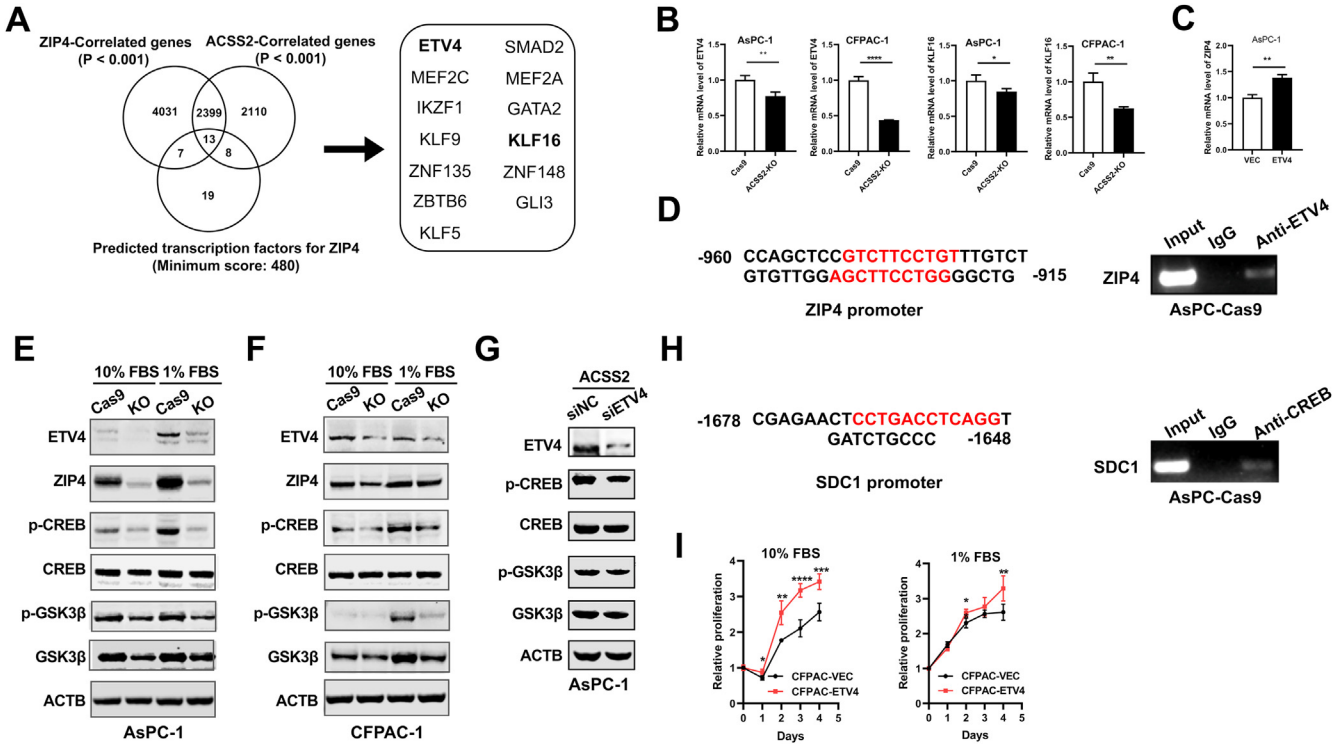

Figure 4. ACSS2 promotes macropinocytosis through the ETV4/ZIP4/CREB pathway. (*A*) Venn diagram shows the candidates of transcription factors for ZIP4. (*B*) mRNA level of ETV4 and KLF16 in ACSS2-KO cell lines. (*C*) mRNA level of ZIP4 in ETV4-overexpression AsPC-1 cells. VEC, vector. (*D*) Predicted binding site of ETV4 on ZIP4 promoter region (*left panel*). ChIP assay to evaluate ETV4 binding to the promoter region of ZIP4 (*right panel*). (*E–F*) Protein level of ETV4, ZIP4, phosphorylated (p)-GSK3β, total-GSK3β, p-CREB, and total-CREB in ACSS2-KO cell lines in 10% FBS or 1% FBS. (*G*) Protein level of ETV4, p-GSK3β, total-GSK3β, p-CREB, and total-CREB in ETV4-knockdown and ACSS2-overexpression cell lines. si, small interfering; (*H*) Predicted binding site of CREB on SDC1 promoter region (*left panel*). ChIP assay to evaluate CREB binding to the promoter region of SDC1 (*right panel*). (*I*) Cell proliferation was assessed by MTT assay in ETV4-overexpression cell lines in 10% FBS or 1% FBS. *$P < .05$, **$P < .01$, ***$P < .001$, **** $P < .0001$.

Knockdown of ETV4 downregulated the phosphorylation of GSK3β and CREB in AsPC-1 cells but not in CFPAC-1 cells (Figure 4*G* and Supplementary Figure 7N and *O*). We previously showed that ZIP4 promotes pancreatic cancer progression by activating CREB.[21] SDC1 is a downstream target of CREB.[22] To examine whether CREB can transcriptionally activate SDC1 in pancreatic cancer, we performed ChIP assay and validated that CREB can bind to the promoter region of SDC1 in pancreatic cancer cells (Figure 4*H*). Overexpression of ETV4 promoted cell proliferation in pancreatic cancer (Figure 4*I*). Knockdown of ETV4, SDC1, and DNM2 decreased macropinocytosis and cell proliferation (Supplementary Figure 8A and *B*). Taken together, these results indicate that ACSS2 promotes macropinocytosis by upregulating macropinocytosis-associated genes, such as *SDC1* and *DNM2*, which are activated through the ZIP4/CREB pathway.

ACSS2 Knockout Suppresses Tumor Growth in Orthotopic Xenograft Mouse Models

To validate the role of ACSS2 in vivo, we established the orthotopic xenograft mouse models using AsPC-Cas9, AsPC-ACSS2–KO, CFPAC-Cas9, and CFPAC-ACSS2–KO cells (Figure 5*A* and *B* and Supplementary Figure 9*A*). ACSS2 KO suppressed tumor growth in both models. ACSS2 KO in AsPC-1 cells significantly decreased abdominal dissemination and extended overall survival of the mice (55 vs 44 days, $P = .0465$) (Figure 5*C* and *D*). In CFPAC-1 cells, which prefer to disseminate to the wound of incision, ACSS2 KO dramatically suppressed tumor grow on the wound (Supplementary Figure 9*B*). ACSS2 expression is high in the area with metabolic stress, such as necrosis (Figure 5*E* and Supplementary Figure 9*C*). ACSS2-KO tumors showed decreased expression of Ki-67, ZIP4, and macropinocytosis-associated genes (*SDC1* and *DNM2*) (Figure 5*F* and *G* and Supplementary Figure 9*D* and *E*). These data demonstrate that ACSS2 KO suppresses tumor growth in the mouse model, partially through decreasing the expression of macropinocytosis-associated genes and macropinocytosis of tumor cells.

ACSS2 Promotes Muscle Wasting Through the Glycogen Synthase Kinase 3-β/Tumor Necrosis Factor Superfamily Member 10 Pathway

We found that mice xenografted with AsPC-ACSS2–KO tumors showed attenuated weight loss compared with AsPC-Cas9 tumors (Supplementary Figure 10*A*). This

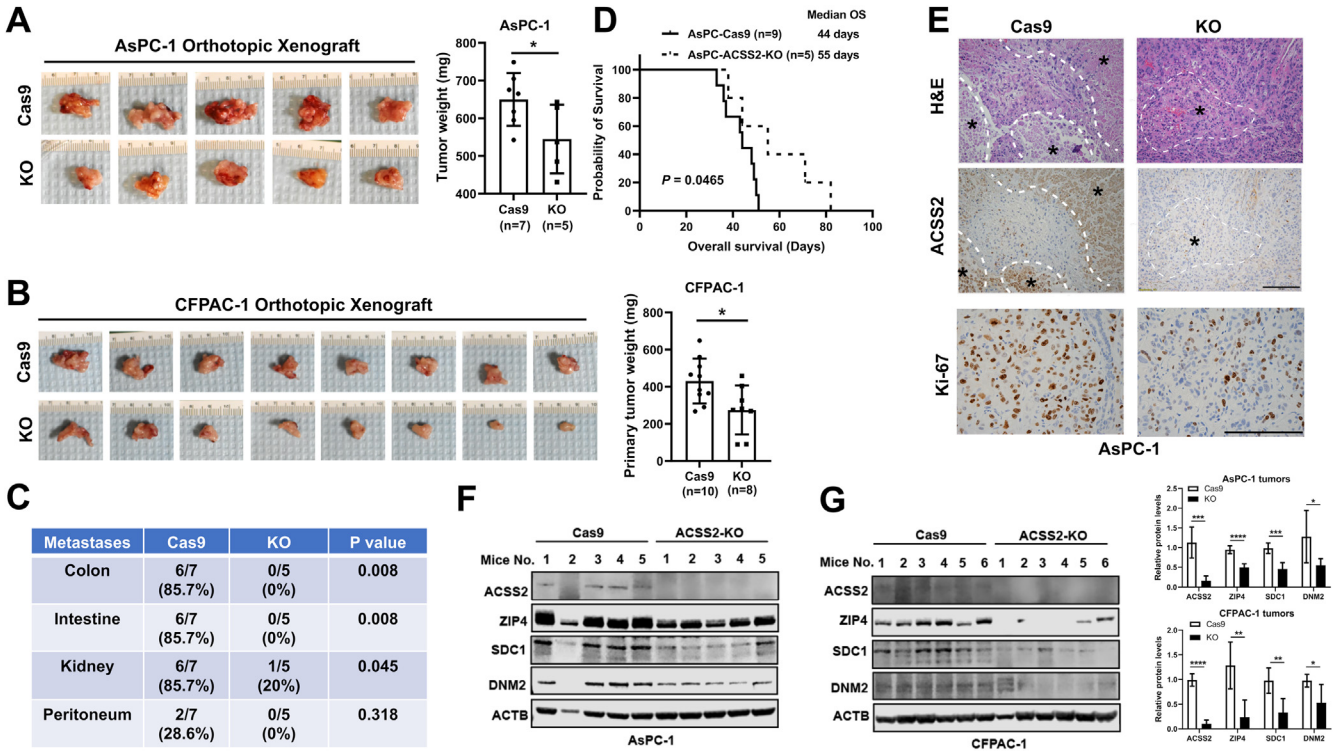

Metastases	Cas9	KO	P value
Colon	6/7 (85.7%)	0/5 (0%)	0.008
Intestine	6/7 (85.7%)	0/5 (0%)	0.008
Kidney	6/7 (85.7%)	1/5 (20%)	0.045
Peritoneum	2/7 (28.6%)	0/5 (0%)	0.318

Figure 5. ACSS2 KO suppresses tumor growth in orthotopic xenograft mouse models. (*A* and *B*) Representative images of tumor mass and tumor weight in pancreatic cancer orthotopic xenograft mouse models. (*C*) Summary of metastases in mice xenografted with AsPC-Cas9 or AsPC-ACSS2–KO tumors. (*D*) Overall survival (OS) of mice xenografted with AsPC-Cas9 or AsPC-ACSS2–KO tumors. (*E*) Representative images of H&E staining, ACSS2, and Ki-67 expression in the xenograft tumor tissue. *Indicates areas with metabolic stress. The *scale bar* is 100 μm. (*F* and *G*) Expression of ACSS2, ZIP4, and macropinocytosis associated genes (SDC1, DNM2) were evaluated in mice tumor tissue. *$P < .05$, **$P < .01$, ***$P < .001$, ****$P < .0001$.

finding prompted us to evaluate the muscle wasting and adipose loss in these mice. We found that ACSS2 KO attenuated muscle wasting and adipose loss (Figure 6*A* and *B* and Supplementary Figure 10*B–D*). Because most cancer cachexia-induced deaths were attributed to muscle wasting, we focused on the role of ACSS2 on muscle wasting. ACSS2 KO attenuated the decrease of muscle grip strength (Figure 6*C*). We evaluated the cross-sectional area of mouse tibialis anterior muscle and gastrocnemius muscle, and found that the ACSS2-KO group had larger cross-sectional area of muscle fibers (Figure 6*D–F* and Supplementary Figure 10*E–G*). ACSS2 KO decreased the expression of muscle wasting markers Atrogin-1 and MuRF1 in mouse muscle tissues (Figure 6*G*).

To explore the underlying mechanism, we established the in vitro muscle differentiation model using the myoblasts C2C12 cells. C2C12 cells were differentiated into myotubes and treated with conditioned medium collected from AsPC-Cas9 or AsPC-ACSS2–KO cells. We found that conditioned medium from ACSS2-KO cells decreased phosphorylation of p38 and suppressed the expression of MuRF-1 and Atrogin-1 in myotubes (Figure 6*H* and *I*, Supplementary Figure 10*H*). Meanwhile, it attenuated the decrease of myosin heavy chain in myotubes (Figure 6*J*). These results indicate that ACSS2 KO reduces muscle wasting in vivo and in vitro.

Next, we explored the mechanism of ACSS2 induced muscle wasting. We examined the expression of several procachexia factors including, TRAIL (TNFSF10), transforming growth factor (TGF)-β, interleukin (IL)1A, and IL1B. We found that ACSS2 KO decreased the transcription of these procachexia factors (Figure 6*K* and *L*). Meanwhile, we also examined the levels of several anticachexia factors, including fibroblast growth factor (FGF) 2 and IL15 (Supplementary Figure 10*I–K*). We found that ACSS2 KO increased the transcription of these anticachexia factors in the pancreatic cancer cells. Overexpression of ACSS2 increased TRAIL and decreased FGF2 mRNA level (Figure 6*M* and Supplementary Figure 10*L*).

We further validated that ACSS2 upregulated the expression of TRAIL in AsPC-1 cells (cachectic cell line) but not in CFPAC-1 cells (noncachectic cell line) (Figure 6*N* and Supplementary Figure 10*M*). ZIP4 knockdown reversed ACSS2-upregulated TRAIL expression and reversed ACSS2-induced muscle wasting (Figure 6*O* and Supplementary Figure 10*N* and *O*). TRAIL expression is lower in ACSS20-KO tumor tissues (Supplementary Figure 10*P*). TRAIL is associated with worse overall survival in patients with pancreatic cancer (median overall survival: 17.0 vs 24.3 months) (Supplementary Figure 10*Q*). The combination of TRAIL and ZIP4 may stratify patients with different prognoses (Figure 6*P*). Those with simultaneously high

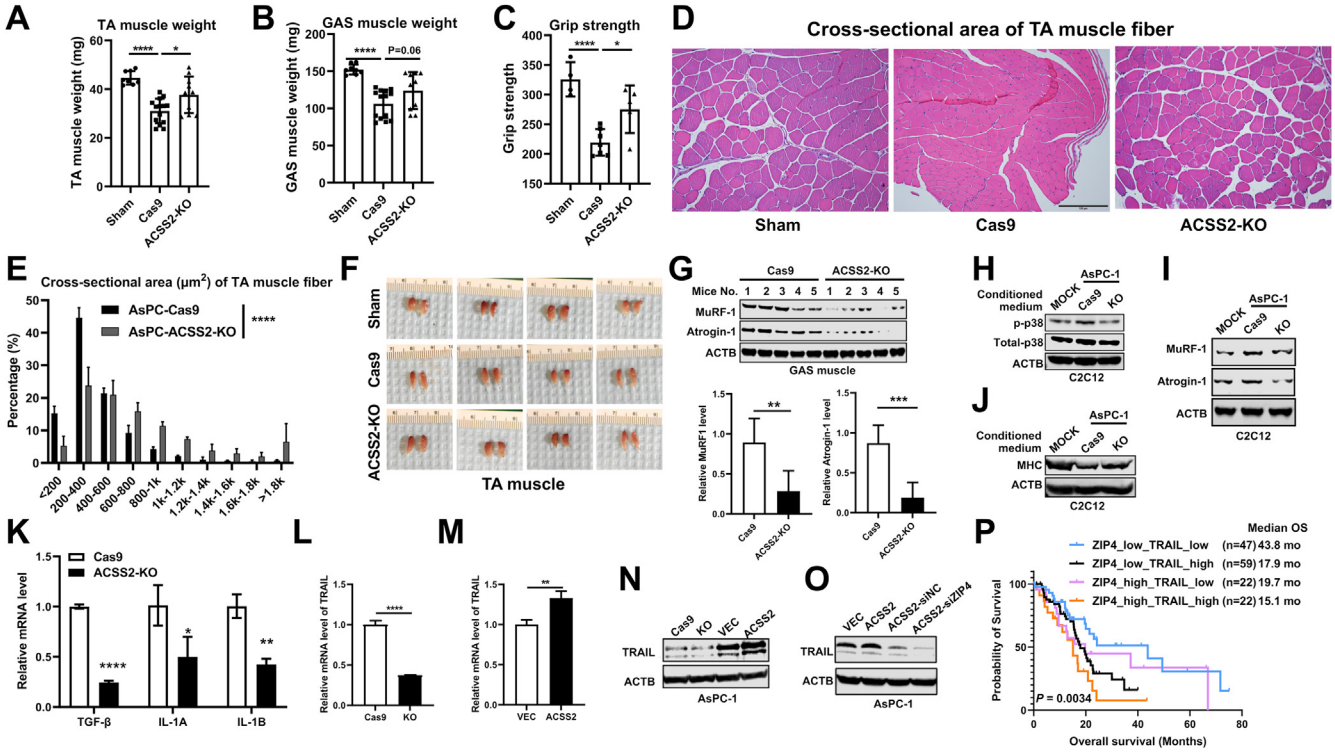

Figure 6. ACSS2 promotes muscle wasting through the GSK3β/TRAIL pathway. Statistics of mouse (*A*) tibialis anterior (TA) muscle weight and (*B*) gastrocnemius (GAS) muscle weight. (*C*) Muscle grip strength of the mice. (*D*) Representative images of H&E staining of cross-sectional area of TA muscle fiber in sham, AsPC-Cas9, and AsPC-ACSS2–KO groups. The *scale bar* is 100 μm. (*E*) Statistical result of cross-sectional area of TA muscle fiber in sham, AsPC-Cas9, and AsPC-ACSS2–KO tumor. (*F*) Representative images of TA muscle in xenograft mouse models. (*G*) Protein levels of atrogin-1 and MuRF1 in mice GAS muscle tissue. (*H–J*) Protein levels of phosphorylated (p)-p38, total-p38, MuRF-1, atrogin-1, and myosin heavy chain (MHC) in C2C12 myotubes treated with conditioned medium from AsPC-Cas9 or AsPC-ACSS2–KO cell lines. (*K*) mRNA level of pro-cachexia markers in ACSS2-KO cell lines. (*L–N*) Protein and mRNA level of TRAIL in ACSS2-KO and ACSS2-overexpressing AsPC-1 cells. (*O*) Protein level of TRAIL in ACSS2 vector or ACSS2-overexpressing AsPC-1 cells transfected with small interfering (si) negative control (NC) or siZIP4 siRNA. (*P*) Survival analysis of pancreatic cancer in TCGA cohort (n = 150) based on TRAIL and ZIP4 expression. *$P < .05$, **$P < .01$, *** $P < .001$, **** $P < .0001$.

expression of TRAIL and ZIP4 had worst prognoses (median overall survival: 15.1 months), whereas those with simultaneously low expression of TRAIL and ZIP4 had the best prognoses (median overall survival: 43.8 months).

Discussion

Our current study found that KO of ACSS2 can suppress cell proliferation in 2- and 3D models in vitro and suppress tumor metastasis and cachexia in vivo. Mechanism study showed that ACSS2 promotes macropinocytosis of tumor cells via ETV4/ZIP4/CREB-mediated reprogramming of macropinocytosis-associated genes. Meanwhile, ZIP4 promotes muscle wasting through the GSK3β/TRAIL axis, which in turn provides additional nutrients to maintain tumor fitness (Figure 7). ACSS2 can induce autophagy of tumor cells under nutritional stress, such as glucose deprivation, via regulating histone acetylation in glioblastoma.[23] Meanwhile, previous studies showed that KO of ACSS2 can suppress tumorigenesis in liver cancer.[24] In c-myc–overexpressing and PTEN-deleted murine model of liver cancer, ACSS2 KO can significantly reduce the incidence of liver cancers.[24]

The roles of ACSS2 in pancreatic cancer tumorigenesis and progression remain poorly defined. ACSS2 is the downstream target of sterol regulatory element-binding protein 2 (SREBP2), which was activated when tumor cells exposed to acidic tumor microenvironment.[25] ACSS2 is highly expressed in pancreatic intraepitheliel neoplasia lesions and in pancreatic cancer tissue, but its role in regulating metabolic reprogramming in pancreatic cancer remains uncharacterized.[12] Management of cachexia remains an unmet need for most gastrointestinal cancers, especially pancreatic cancer. The systematic reprogramming of metabolic profiles drives cancer cachexia to provide nutrients to support tumor growth.[1]

Macropinocytosis is a nonselected protein scavenging process critical for tumor progression, especially for KRAS-mutant tumors, such as pancreatic cancer, which is characterized with desmoplasia and nutrient deficiency.[6,26] KRAS mutation can upregulate macropinocytosis, which provides an essential supply of amino acids for tumor growth in a nutrient-deficient microenvironment. Tumor cells under metabolic stress upregulate macropinocytosis through metabolic reprogramming. For instance, glutamine deficiency upregulates macropinocytosis to maintain amino

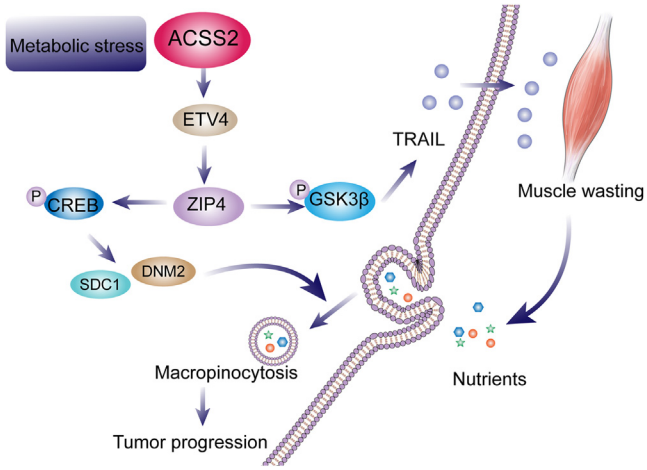

Figure 7. Schematic diagram of ACSS2-mediated macropinocytosis and cancer cachexia in pancreatic cancer. ACSS2 promotes metabolic reprogramming through the ETV4/ZIP4 pathway, whereby ZIP4 promotes macropinocytosis via SDC1/DNM2 and drives muscle wasting through the GSK3β/TRAIL axis, which in turn provides additional nutrients for macropinocytosis in pancreatic cancer.

acid supply in pancreatic cancer.[27] ACSS2 expression in tumor cells was increased when glucose or serum in the culture medium was deficient, indicating tumor cells reprogramed the metabolic profiles to maintain fitness under a nutrient-deficient microenvironment. We found that a nutrient-deficient microenvironment can upregulate ACSS2 in pancreatic cancer.

We explored the mechanism of ACSS2-increased macropinocytosis in pancreatic cancer and identified a zinc transporter ZIP4 as a downstream target of ACSS2. ZIP4 can promote cancer cachexia, gemcitabine resistance, and epithelial-mesenchymal transition in pancreatic cancer.[15,28–30] We found that ACSS2 upregulates ZIP4 through ETV4-mediated transcriptional activation and then explored how ZIP4 regulates macropinocytosis. Studies showed that pancreatic cancer upregulates macropinocytosis via SDC1 and epidermal growth factor receptor pathways.[27,31]

To evaluate the role of ACSS2 in mediating macropinocytosis, we analyzed the correlation between ACSS2 and macropinocytosis-associated genes. We found that ACSS2 can upregulate macropinocytosis by increasing the expression of macropinocytosis-associated genes such as *SDC1* and *DNM2*. Knockdown of ZIP4 can reverse ACSS2-induced macropinocytosis. The phosphatidylinositol-3-kinase–protein kinase B (AKT) pathway is critical for RAS-induced macropinocytosis.[32] We found that ACSS2 can induce the phosphorylation of GSK3β and CREB, which is partially dependent on ZIP4. CREB can bind to the promoter region of SDC1 (cluster of differentiation 138). Another study showed that the GSK3β pathway promotes endocytosis by activating dynamin 1.[33] This is consistent with our findings showing that ACSS2 can promote macropinocytosis.

Intriguingly, we found that the impact of ZIP4 downregulation on macropinocytosis is not as substantial as ACSS2 downregulation, indicating additional downstream mediators of ACSS2 may also play important roles on macropinocytosis, which may be independent of ZIP4. Downregulation of ZIP4 has a more dramatic effect on pancreatic cancer proliferation than macropinocytosis, suggesting the potential cell-autonomous effects of ZIP4 downregulation that go beyond macropinocytosis, such as ZIP4-mediated microRNA-373 and equilibrative nucleoside transporter 1 pathways.[16,21,29] Together, the evidence above demonstrates that metabolic stress can upregulate ACSS2, which promotes macropinocytosis via the ZIP4/CREB/SDC1 pathway to support tumor growth.

On the other side, we found that ACSS2 KO can attenuate body weight loss, adipose loss, and muscle wasting, all of which are characteristics of cancer cachexia. Cancer-induced metabolic reprogramming is believed to be the driving force of tissue catabolism and imbalanced energy expenditure in cachexia.[2] Cancer-derived circulating factors have garnered substantial attention in the field of cachexia in the past decade, including the TGF-β superfamily (Hsp70/90, activin A, TGF-β, myostatin, and growth/differentiation factor 15),[16,34,35] tumor necrosis factor superfamily,[36] IL6,[37] and leukemia inhibitory factor,[38] etc. These procachexia factors are involved in integrated alterations on metabolism. For example, growth/differentiation factor 15 induced anorexia and lipolysis by interacting with central nervous system and adipose tissue.[34] IL6 induced cachexia by orchestrating the cross talk between muscle and adipose tissue.[37]

Nonetheless, the molecular mechanism of pancreatic cancer-induced cachexia, especially muscle wasting, remains poorly understood. Emerging evidence showed that pancreatic cancer cells induced muscle atrophy by secreting TGF-β and IL6, etc.[16,37] These cytokines induce muscle atrophy by activating atrogin-1 (FBX032) and MuRF1 (TRIM63)–mediated muscle fiber degradation.[30] Our study found that ACSS2-KO cells reduced the levels of several procachexia factors, including IL1A, IL1B, TGF-β, and TRAIL. Meanwhile, the levels of several anticachexia factors were increased in the ACSS2-KO pancreatic cancer cells, including FGF2 and IL15. These results indicate ACSS2 can reprogram the metabolic profiles of pancreatic cancer cells to induce cachexia. Among these factors, we are particularly interested in TRAIL (also known as TNFSF10). TRAIL is a member of the tumor necrosis factor superfamily, which is correlated to cachexia in pancreatic cancer.[39] Knockdown of ZIP4 can reverse ACSS2-induced TRAIL expression. Furthermore, we found that TRAIL expression is associated with worse overall survival of patients. The combination of ZIP4 and TRAIL can stratify patients with different prognoses more precisely. We found that ACSS2 can induce phosphorylation of GSK3β at Ser9 and thus inhibits the activity of GSK3β. Emerging evidence showed that macropinocytosis can induce phosphorylation of AKT, which would lead to increased cell proliferation and resistance to mechanistic target of rapamycin inhibition in KRAS-driven pancreatic cancer.[40] Given that AKT can induce phosphorylation of GSK3β, the latter of which would upregulate TRAIL, we speculated that macropinocytosis may also promote cancer cachexia. Specifically, to meet the high demand of nutrients, tumor cells rewired

their metabolic profiles to induce cancer cachexia. The degraded muscle fibers and adipose tissue could provide tumor cells with additional nutrients needed for tumor growth, forming a feedforward loop. Further studies are warranted to address the cross talk between macropinocytosis and cachexia.

In summary, our study describes a previously uncharacterized role of ACSS2 in dominating metabolic reprogramming in pancreatic cancer. ACSS2 increases macropinocytosis to support tumor progression and promotes cancer cachexia to provide nutrients for tumor growth. Specifically, ACSS2 promotes metabolic reprogramming through the ETV4/ZIP4 pathway, whereby ZIP4 promotes macropinocytosis via the CREB-activated SDC1/DNM2 pathway and drives muscle wasting through the GSK3β/TRAIL-signaling axis, which fuels back the tumor cells to provide additional nutrients to maintain tumor fitness in pancreatic cancer. These results indicate that ACSS2 is an attractive vulnerability for the treatment of cachexia induced by pancreatic cancer.

Supplementary Material

Note: To access the supplementary material accompanying this article, visit the online version of *Gastroenterology* at www.gastrojournal.org, and at https://dx.doi.org/10.1053/j.gastro.2022.06.058.

References

1. Baracos VE, Martin L, Korc M, et al. Cancer-associated cachexia. Nat Rev Dis Primers 2018;4:17105.
2. Argiles JM, Stemmler B, Lopez-Soriano FJ, et al. Inter-tissue communication in cancer cachexia. Nat Rev Endocrinol 2018;15:9–20.
3. Huot JR, Pin F, Narasimhan A, et al. ACVR2B antagonism as a countermeasure to multi-organ perturbations in metastatic colorectal cancer cachexia. J Cachexia Sarcopenia Muscle 2020;11:1779–1798.
4. Roeland EJ, Bohlke K, Baracos VE, et al. Management of cancer cachexia: ASCO Guideline. J Clin Oncol 2020;38:2438–2453.
5. Wood LD, Canto MI, Jaffee EM, et al. Pancreatic cancer: pathogenesis, screening, diagnosis, and treatment. Gastroenterology 2022;163:386–402.e1.
6. **Kamphorst JJ, Nofal M, Commisso C**, et al. Human pancreatic cancer tumors are nutrient poor and tumor cells actively scavenge extracellular protein. Cancer Res 2015;75:544–553.
7. Hosein AN, Brekken RA, Maitra A. Pancreatic cancer stroma: an update on therapeutic targeting strategies. Nat Rev Gastroenterol Hepatol 2020;17:487–505.
8. **Ramirez C, Hauser AD**, Vucic EA, et al. Plasma membrane V-ATPase controls oncogenic RAS-induced macropinocytosis. Nature 2019;576:477–481.
9. **Schug ZT, Peck B**, Jones DT, et al. Acetyl-CoA synthetase 2 promotes acetate utilization and maintains cancer cell growth under metabolic stress. Cancer Cell 2015;27:57–71.
10. **Mashimo T, Pichumani K**, Vemireddy V, et al. Acetate is a bioenergetic substrate for human glioblastoma and brain metastases. Cell 2014;159:1603–1614.
11. Luong A, Hannah VC, Brown MS, et al. Molecular characterization of human acetyl-CoA synthetase, an enzyme regulated by sterol regulatory element-binding proteins. J Biol Chem 2000;275:26458–26466.
12. Carrer A, Trefely S, Zhao S, et al. Acetyl-CoA metabolism supports multistep pancreatic tumorigenesis. Cancer Discov 2019;9:416–435.
13. **Slaymaker IM, Gao L**, Zetsche B, et al. Rationally engineered Cas9 nucleases with improved specificity. Science 2016;351:84–88.
14. **Joung J, Konermann S**, Gootenberg JS, et al. Genome-scale CRISPR-Cas9 knockout and transcriptional activation screening. Nat Protoc 2017;12:828–863.
15. **Liu M, Zhang Y, Yang J**, et al. Zinc-dependent regulation of ZEB1 and YAP1 coactivation promotes epithelial-mesenchymal transition plasticity and metastasis in pancreatic cancer. Gastroenterology 2021;160:1771–1783.e1.
16. **Shi X, Yang J, Liu M**, et al. Circular RNA ANAPC7 inhibits tumor growth and muscle wasting via PHLPP2-AKT-TGF-β signaling axis in pancreatic cancer. Gastroenterology 2022;162:2004–2017.e2.
17. **Zhou Z, Xia G, Xiang Z**, et al. A C-X-C chemokine receptor type 2-dominated cross-talk between tumor cells and macrophages drives gastric cancer metastasis. Clin Cancer Res 2019;25:3317–3328.
18. Commisso C, Flinn RJ, Bar-Sagi D. Determining the macropinocytic index of cells through a quantitative image-based assay. Nat Protoc 2014;9:182–192.
19. **Durbin AD, Wang T**, Wimalasena VK, et al. EP300 selectively controls the enhancer landscape of MYCN-amplified neuroblastoma. Cancer Discov 2022;12:730–751.
20. Mews P, Donahue G, Drake AM, et al. Acetyl-CoA synthetase regulates histone acetylation and hippocampal memory. Nature 2017;546:381–386.
21. **Zhang Y, Yang J, Cui X**, et al. A novel epigenetic CREB-miR-373 axis mediates ZIP4-induced pancreatic cancer growth. EMBO Mol Med 2013;5:1322–1334.
22. Kim C, Wilcox-Adelman S, Sano Y, et al. Antiinflammatory cAMP signaling and cell migration genes coopted by the anthrax bacillus. Proc Natl Acad Sci U S A 2008;105:6150–6155.
23. Li X, Yu W, Qian X, et al. Nucleus-translocated ACSS2 promotes gene transcription for lysosomal biogenesis and autophagy. Mol Cell 2017;66:684–697.e9.
24. **Comerford SA, Huang Z**, Du X, et al. Acetate dependence of tumors. Cell 2014;159:1591–1602.
25. Kondo A, Yamamoto S, Nakaki R, et al. Extracellular acidic pH activates the sterol regulatory element-binding protein 2 to promote tumor progression. Cell Rep 2017;18:2228–2242.
26. Su H, Yang F, Fu R, et al. Cancer cells escape autophagy inhibition via NRF2-induced macropinocytosis. Cancer Cell 2021;39:678–693.e11.
27. Lee SW, Zhang Y, Jung M, et al. EGFR-Pak signaling selectively regulates glutamine deprivation-induced macropinocytosis. Dev Cell 2019;50:381–392.e5.

28. Liu M, Yang J, Zhang Y, et al. ZIP4 promotes pancreatic cancer progression by repressing ZO-1 and claudin-1 through a ZEB1-dependent transcriptional mechanism. Clin Cancer Res 2018;24:3186–3196.
29. **Liu M, Zhang Y, Yang J**, et al. ZIP4 increases expression of transcription factor ZEB1 to promote integrin $\alpha 3\beta 1$ signaling and inhibit expression of the gemcitabine transporter ENT1 in Pancreatic Cancer Cells. Gastroenterology 2020;158:679–692.e1.
30. **Yang J, Zhang Z, Zhang Y**, et al. ZIP4 promotes muscle wasting and cachexia in mice with orthotopic pancreatic tumors by stimulating RAB27B-regulated release of extracellular vesicles from cancer cells. Gastroenterology 2019;156:722–734.e6.
31. Yao W, Rose JL, Wang W, et al. Syndecan 1 is a critical mediator of macropinocytosis in pancreatic cancer. Nature 2019;568:410–414.
32. Amyere M, Payrastre B, Krause U, et al. Constitutive macropinocytosis in oncogene-transformed fibroblasts depends on sequential permanent activation of phosphoinositide 3-kinase and phospholipase C. Mol Biol Cell 2000;11:3453–3467.
33. **Reis CR, Chen PH**, Srinivasan S, et al. Crosstalk between Akt/GSK3β signaling and dynamin-1 regulates clathrin-mediated endocytosis. EMBO J 2015;34:2132–2146.
34. **Suriben R, Chen M, Higbee J**, et al. Antibody-mediated inhibition of GDF15-GFRAL activity reverses cancer cachexia in mice. Nat Med 2020;26:1264–1270.
35. Loumaye A, de Barsy M, Nachit M, et al. Circulating activin A predicts survival in cancer patients. J Cachexia Sarcopenia Muscle 2017;8:768–777.
36. Johnston AJ, Murphy KT, Jenkinson L, et al. Targeting of Fn14 prevents cancer-induced cachexia and prolongs survival. Cell 2015;162:1365–1378.
37. Rupert JE, Narasimhan A, Jengelley DHA, et al. Tumor-derived IL-6 and trans-signaling among tumor, fat, and muscle mediate pancreatic cancer cachexia. J Exp Med 2021;218:e20190450.
38. Kandarian SC, Nosacka RL, Delitto AE, et al. Tumour-derived leukaemia inhibitory factor is a major driver of cancer cachexia and morbidity in C26 tumour-bearing mice. J Cachexia Sarcopenia Muscle 2018;9:1109–1120.
39. Freire PP, Fernandez GJ, de Moraes D, et al. The expression landscape of cachexia-inducing factors in human cancers. J Cachexia Sarcopenia Muscle 2020;11:947–961.
40. Michalopoulou E, Auciello FR, Bulusu V, et al. Macropinocytosis renders a subset of pancreatic tumor cells resistant to mTOR inhibition. Cell Rep 2020;30:2729–2742.e4.

Author names in bold designate shared co-first authorship.

Received April 20, 2022. Accepted June 17, 2022.

Correspondence
Address correspondence to: Min Li, PhD, Department of Medicine, Department of Surgery, The University of Oklahoma Health Sciences Center, 975 Northeast 10th Street, BRC 1262A, Oklahoma City, Oklahoma 73104. e-mail: Min-Li@ouhsc.edu; or Courtney W. Houchen, MD, Department of Medicine, The University of Oklahoma Health Sciences Center, 800 Stanton L. Young Boulevard, Oklahoma City, Oklahoma 73104. e-mail: courtney-houchen@ouhsc.edu; or Yuqing Zhang, PhD, Department of Medicine, The University of Oklahoma Health Sciences Center, 975 Northeast 10th Street, BRC 1215A, Oklahoma City, Oklahoma 73104. e-mail: Yuqing-Zhang@ouhsc.edu.

CRediT Authorship Contributions
Zhijun Zhou, MD (Conceptualization: Lead; Data curation: Lead; Formal analysis: Lead; Software: Lead; Visualization: Lead; Writing – original draft: Lead).

Yu Ren, PhD (Data curation: Equal; Investigation: Equal; Methodology: Equal; Project administration: Supporting; Resources: Equal; Software: Equal; Visualization: Lead; Writing – review & editing: Lead).

Jingxuan Yang, PhD (Investigation: Equal; Methodology: Lead; Project administration: Lead; Resources: Lead; Supervision: Lead; Writing – review & editing: Lead).

Mingyang Liu, MD, PhD (Conceptualization: Equal; Formal analysis: Equal; Investigation: Equal; Methodology: Lead; Resources: Lead; Validation: Equal; Writing – review & editing: Equal).

Xiuhui Shi, MD, PhD (Data curation: Equal; Formal analysis: Equal; Investigation: Equal; Methodology: Equal; Project administration: Supporting; Visualization: Equal).

Wenyi Luo, MD, PhD (Formal analysis: Supporting; Investigation: Supporting; Methodology: Supporting; Resources: Supporting; Visualization: Supporting).

Kar-Ming Fung, MD, PhD (Investigation: Supporting; Methodology: Supporting; Resources: Supporting; Software: Supporting).

Chao Xu, PhD (Methodology: Supporting; Resources: Supporting; Software: Supporting).

Michael Bronze, MD (Investigation: Supporting; Project administration: Supporting; Resources: Supporting; Supervision: Supporting).

Yuqing Zhang, PhD (Methodology: Equal; Project administration: Equal; Resources: Lead; Supervision: Equal; Writing – review & editing: Lead).

Courtney Houchen, MD (Methodology: Equal; Project administration: Equal; Resources: Equal; Supervision: Lead).

Min Li, PhD (Conceptualization: Lead; Funding acquisition: Lead; Methodology: Lead; Resources: Lead; Supervision: Lead; Writing – review & editing: Lead).

Conflicts of interest
This author discloses the following: Courtney W. Houchen has ownership interest in COARE Holdings Inc. The remaining authors disclose no conflicts.

Funding
This work was supported in part by National Institutes of Health National Cancer Institute grants R01 CA186338, R01 CA203108, R01 CA247234, and award P30 CA225520, and by the William and Ella Owens Medical Research Foundation (Min Li).

Supplementary Materials and Methods

C2C12 Myogenic Cell Culture

Murine C2C12 myoblasts (from the American Type Culture Collection) were cultured in normal growth medium (Dulbecco's modified Eagle medium with 10% FBS) at 37°C under 5% CO_2. The myoblast differentiation was induced when the culture of C2C12 cells reaches 85% to 90% confluence, by incubation in differentiation medium (Dulbecco's modified Eagle medium supplemented with 2%–4% horse serum) for 72 hours to 96 hours to let the C2C12 cells fuse into multinucleated syncytium, as myotubes. Then the conditioned medium from cultures of pancreatic carcinoma cell lines (48–72 hours) were centrifuged to remove floating cells and added to C2C12 myotube cultures (25% final volume in fresh medium) when indicated. The conditioned medium was replaced every 24 hours, and the myotubes were collected at designated incubation times for Western blot analysis with antibodies against certain cachexia markers.

Single-Cell Transcriptomic Analysis

Single-cell transcriptomic data of normal pancreas and pancreas from early-stage (40-day-old) and late-stage (60-day-old) $Kras^{LSL-G12D/+}Ink4a^{fl/fl}Ptf1a^{Cre/+}$ (*KIC*) and 6-month-old $Kras^{LSL-G12D/+}Trp53^{LSL-R172H/+}Ptf1a^{Cre/+}$ (*KPC*) mice models were obtained from GSE125588.[1] Data were analyzed in Seurat 4.0 (New York Genome Center, New York, NY).[2] Cells with feature counts of <200 or >2500 and those with $>5\%$ mitochondria counts were filtered, followed by the normalization of the data. Uniform manifold approximation and projection nonlinear dimensional reduction was applied to visualize the population of the cells.

Polymerase Chain Reaction

PCR was performed using the FastStart Taq DNA Polymerase kit (Roche), following the manufacturer's instructions. Primers were synthesized by Sigma-Aldrich (St Louis, MO). The reaction was performed with an Eppendorf thermal cycler.

Human Tissue Samples

Human pancreatic cancer tissue samples and information on body weight loss were obtained from the University of Oklahoma Health Sciences Center. The Institutional Review Board approved this study. Written consents were collected from all patients. Deidentified tissue samples were used for the study.

Colony Formation Assay

Cells were seeded on 3-cm dish (500–2000 cells/dish dependent on cell lines). The dish was replaced with new culture medium every 48 hours. The cells were allowed to grow for 10 to 15 days. Cells were then fixed with 3.7% formaldehyde in PBS for 15 minutes at room temperature, followed by staining with 0.5% crystal violet for 30 minutes at room temperature. The colonies were scanned and analyzed by ImageJ.

Database Analysis

Transcriptomic data and clinical information of patients with pancreatic cancer were obtained from TCGA (https://portal.gdc.cancer.gov/), cBioPortal (https://www.cbioportal.org/), Gene Expression Omnibus (GEO) (https://www.ncbi.nlm.nih.gov/geo/), and Gene Expression Profiling Interactive Analysis (GEPIA) 2.0 database (http://gepia2.cancer-pku.cn/). The RNA sequencing data were transformed by $\log_2$ and analyzed as previously described.[3] Transcriptomic data of cancer cell lines were obtained from the Dependency Map (DepMap) portal (https://depmap.org/portal/). Because these are publicly available databases and all patients' personal information have been deidentified, patients' consent and ethic approval were waived by the institutional ethics committee.

Supplementary References

1. Hosein AN, Huang H, Wang Z, et al. Cellular heterogeneity during mouse pancreatic ductal adenocarcinoma progression at single-cell resolution. JCI Insight 2019;5:e129212.
2. Hao Y, Hao S, Andersen-Nissen E, et al. Integrated analysis of multimodal single-cell data. Cell 2021;184:3573–3587.e29.
3. Zhou Z, Zhang J, Xu C, et al. An integrated model of N6-methyladenosine regulators to predict tumor aggressiveness and immune evasion in pancreatic cancer. EBioMedicine 2021;65:103271.